J Mater Sci (2009) 44:1741–1749
DOI 10.1007/s10853-008-3191-z

Effect of dopants on alumina grain boundary sliding: implications for creep inhibition

Ivan Milas · Emily A. Carter

Received: 1 June 2008 / Accepted: 12 December 2008 / Published online: 22 January 2009

Abstract We investigate by means of periodic density functional theory the mechanism of grain boundary sliding along the α-alumina Σ11 tilt grain boundary. We identify minimum and maximum energy structures along a preferential sliding pathway for the pure grain boundary, as well as for grain boundaries doped with a series of early transition metals, as well as barium, gadolinium, and neodymium. We predict that the segregation of those dopants results in a considerable increase in the grain boundary sliding barrier. Grain boundary sliding occurs by a series of bond breaking and forming across the grain boundary. Our results suggest that the presence of large cations inhibits the regeneration of bonds during sliding, which results in a decrease in total number of bonds across the grain boundary interface, thereby raising the barrier to sliding. Trends in predicted grain boundary sliding energies are in good agreement with recently measured creep activation energies in polycrystalline alumina, lending further credence to the notion that grain boundary sliding plays a dominant role in alumina creep.

Introduction

Application of thermal barrier coatings (TBCs) to Ni-based superalloy jet engine components allows the engines to operate at temperatures higher than the melting point of the superalloy [1]. In a typical three-layer TBC, a NiAl-based bond coat alloy is deposited on the Ni superalloy substrate to improve TBC adhesion. Thermal protection is provided by the yttria-stabilized zirconia (YSZ) topcoat. Finally, a thin layer of a thermally grown oxide (TGO) between the topcoat and the bond coat protects the superalloy from oxidative corrosion, since oxygen readily diffuses through the YSZ layer. Alumina's low oxygen mobility and relatively slow oxide growth even at high temperatures make it optimal as a TGO.

Unfortunately, alumina's coefficient of thermal expansion (CTE) is considerably lower than that of the underlying metal alloys. Upon thermal cycling of the engine, the CTE mismatch causes stress to accumulate in the growing oxide layer. Once the thickness of the oxide reaches a critical value (around 10 μm), the stresses become so large that they must be alleviated by either creep or plastic deformation, which leads to failure of the coating [2]. Thus, TBC lifetime can be extended by either slowing oxide growth or by increasing its creep resistance. In this work, we focus on considering avenues to increase creep resistance.

The creep rate generally can be expressed by the following equation:

$$\frac{d\varepsilon}{dt} = CD_0 e^{-Q/kT}(\sigma^n/d^p)$$

where ε is the creep strain, C is a constant, Q is the creep activation energy, D_0 is the pre-exponential factor, d is the grain size, σ is the stress, p is the grain size exponent, and n is the stress exponent. The values of p and n are dependent on the creep mechanism involved. The data obtained for high temperature creep in polycrystalline alumina are consistent with a value of 3 for the grain size exponent [3, 4], which usually indicates Coble creep [5]. In this mechanism, the stress build-up in alumina produces an excess of

I. Milas · E. A. Carter (✉)
Department of Mechanical and Aerospace Engineering and Program in Applied and Computational Mathematics, Princeton University, Princeton, NJ 08544-5263, USA
e-mail: eac@princeton.edu

vacancies along grain boundaries (GBs) experiencing tensile stress and depletion of vacancies at GBs under compressive stress. This in turn causes a diffusive flow of atoms from regions under compressive stress to regions under tensile stress [6]. This process leads to grain elongation along the tensile axis. Elongation of grains has been observed during isothermal oxidation of α-alumina scales on Y-doped NiCrAl-based bond coats [7], but this effect has been attributed to the inward growth of the oxide rather than diffusional creep.

Coble creep mechanisms are known to exhibit a stress exponent of 1. Instead the stress exponent for polycrystalline alumina is found to be 2, which is characteristic of GB sliding [8] or interface-reaction-controlled creep [9]. However, these mechanisms require a grain exponent of 2 and not the value 3 observed in this case. In an attempt to reconcile this disparity, an alternative creep mechanism based on empirical observations has been proposed [10, 11], which involves GB sliding as a first step, followed by a movement of dislocations to offset any accumulated voids [12, 13]. The grains in this mechanism retain their original shapes (usually equiaxial). Equiaxial grains are usually observed when the α-alumina scale is grown on NiAl-based bond coats [14]. However, the shape of the grains alone cannot be taken as the indicator of the type of creep mechanism involved, because at high temperatures concurrent grain growth and rearrangements can result in an equiaxial shape of grains, despite the dominant mechanism being diffusion creep [15]. This model, despite fitting the available experimental creep data well, is purely phenomenological and no rigorous derivation of its associated equations has been put forth.

Some recent data indicate that diffusion alone cannot be rate-limiting step for creep in alumina. Bedu-Amissah et al. [16] estimated Al diffusion barriers in pure and doped alumina by using a Cr tracer and by assuming that Al and Cr diffusion barriers would be the same. The activation energy for Cr diffusion in pure alumina is 2.64 ± 0.49 eV and in Y-doped alumina is 2.95 ± 0.44 eV. Cheng et al. [17] studied the O diffusion in alumina by using Ni particles as markers. They determined that the activation energy for O diffusion in pure alumina is 4.46 ± 0.44 eV and is 5.15 ± 0.08 eV for Y-doped alumina. These values are lower than the activation energies for creep in pure and Y-doped alumina found by the same group (5.0 eV and 7.1 eV, respectively [3]) and the authors concluded that additional processes with higher activation energies must be involved in creep.

Yttrium and some other early transition metal dopants, also known as reactive elements (REs), have been shown to significantly reduce both oxide growth and creep rates in alumina [14, 18]. The increase of alumina's creep resistance by the addition of REs is commonly thought to be due solely to blocking diffusion pathways at GBs. However, recently Matsunaga et al. [19] performed creep experiments on pure and doped alumina bicrystals in which they limited diffusion creep, and thus their creep rates depended almost entirely on GB sliding barriers. They observed that the creep rate of bicrystals doped with Y was two orders of magnitude lower than the one found for pure bicrystals. These findings show that the role of REs in increasing creep resistance is not limited to site-blocking along diffusion pathways, but must also involve their ability to hinder GB sliding [20, 21].

Since in situ experimental observations of creep at temperatures that exceed 1000 °C are rare and have become possible only recently with the use of synchrotron light [22], the use of simulation techniques can help elucidate the mechanisms that occur under these conditions. Our focus here is on GB sliding mechanisms only, with diffusional creep mechanisms to be considered in future work. To the best of our knowledge, GB sliding in ceramics has been studied only once before using first-principles quantum mechanics. Nakamura et al. [23] used density functional theory within the generalized gradient approximation (DFT-GGA) for electron exchange and correlation to study GB sliding of an undoped Σ13 alumina GB. They assessed the ionicity and covalency of the Al–O bonds across the GB interface and correlated the height of the energy barrier for sliding to the strength of the bonds at the interface.

In the present work, we use all-electron frozen-core projector augmented wave (PAW) DFT-GGA calculations in order to study the structure and electronic properties of pure and doped $\Sigma 11(10\overline{1}\overline{1})\|(10\overline{1}1)$ alumina GBs during the GB sliding process. Although a large number of different GBs form during α-alumina growth, we selected a representative GB to examine in detail. High symmetry GBs such as the Σ11 represent only a very small fraction of the GB population, but we hope that the qualitative insights obtained from a detailed study of one GB may apply more generally. The use of first principles quantum mechanics allows us to explore without assumptions how RE dopants bond across and in the vicinity of the GB, and hence to clarify the causes of the increase in creep resistance experienced by doped alumina.

Calculational details

We perform Kohn–Sham DFT [24, 25] calculations within the Vienna ab initio simulation package (VASP) [26–28], which imposes periodic boundary conditions and employs a plane wave basis. The valence electron–ion interaction, where "ion" refers to the nucleus and core electrons taken together, is described using Blöchl's frozen core PAW

formalism [29], as implemented by Kresse and Joubert [30]. The valence electron distributions of each element are always solved for explicitly, including the valence s and p for Al and O; the valence s and d for all transition metals; the valence s for barium; and the valence 4f, 6s, and 5d for the lanthanides (Nd and Gd). For increased accuracy, the outer core electrons are also treated explicitly as follows: 3p for Sc and Ti, 4s and 4p for Y and Zr, 5s and 5p for Ba and La, and 5p for Hf. The electron exchange and correlation is described by the Perdew–Burke–Ernzerhof (PBE) [31] GGA functional.

Plane wave basis kinetic energy cutoffs of 530 eV for the valence wavefunctions and 610 eV for the augmentation density are used for all calculations. The Brillouin zone is sampled with a Γ-point-centered k-point grid of $1 \times 4 \times 1$, using the Monkhorst–Pack scheme [32], which corresponds to spacings of 0.457, 0.369, and 0.184 Å^{-1} along the a, b, and c reciprocal lattice vectors, respectively. The k-point mesh and the 530 eV/610 eV kinetic energy cutoffs above produce total energies converged to 0.001 eV/atom. The convergence of the total energy with respect to the k-point mesh for alumina is described elsewhere [33]; this mesh is sufficient for convergence of the total energies of the 180+-atom unit cells we employ here.

All results for the pristine GB are obtained by spin-restricted calculations, since all the electrons in alumina are paired and all the structures we consider are stoichiometric, i.e., they contain an integer number of Al_2O_3 formula units. The results for GBs with a reactive element on the GB interface are obtained with spin-polarized calculations, due to the open-shell nature of these dopants. Ion relaxations are performed with a conjugate gradient algorithm and the forces on each atom are converged to 0.03 eV/Å.

To simulate sliding of α-alumina GBs, we use the $\Sigma 11(10\bar{1}\bar{1})\|(10\bar{1}1)$ GB model structure we optimized in previous work [34]. This structure is obtained by further relaxing the model structure for the same GB obtained by Kenway [35], which was based on high resolution transmission electron microscopy images [36]. We use the same surface termination for both sides of the GB interface as in the Kenway model. The optimal positioning of the two grains with respect to each other is found by rigid translation relative to each other, followed by a relaxation of all atoms. Further details on the optimization procedure can be found in Ref. [34]. We obtain a unit cell with lattice vectors of the following magnitudes: $a = 15.537$ Å, $b = 4.809$ Å, and $c = 34.840$ Å, where the lattice vector c includes 10 Å vacuum to isolate periodic images of the GB model. The optimized structure of this GB is shown in Fig. 1a.

Sliding of pristine and Y-doped $\Sigma 11(10\bar{1}\bar{1})\|(10\bar{1}1)$ GBs is simulated by rigidly translating one side of the GB relative to the other side along either of the lattice vectors a and b. The minimum energy structures from Ref. [34] are used as starting GB structures for the calculations in this work. In our previous work, we scanned the GB interface for all possible adsorption sites for Al, O, Y, and Hf atoms. The adsorbed atom is added to the pristine GB model; it is not substituted for an aluminum atom at the GB. The lowest-energy Y adsorption site is used here as the starting structure for translations. First, the $(10\bar{1}1)$ side of the GB is rigidly translated along the a lattice vector at intervals of approximately 0.64 Å. The same procedure is repeated along the b lattice vector at intervals of 0.60 Å. To obtain the full sliding profile along the a vector, it is sufficient to perform the translation on only 1/3 of the length of the vector, because the $(10\bar{1}1)$ side of GB model was constructed by replicating the unit cell three times in the a direction. Further refinements of the translation vector at intervals of 0.3 Å are performed around the peaks in the sliding energy profiles. We do not consider translations of the diagonal $(a + b)$ type, because in Ref. [34] we explored the full potential energy surface by single-point energy calculations (no ion relaxation) for translations of this GB and found that structures obtained by diagonal translations were always much higher in energy than structures obtained by translations along one or the other lattice vector.

After each translation of both the pristine and the Y-doped GB models, the structures are allowed to fully relax, except for the outermost layers of each outer surface, which are frozen to ensure that translated structures do not relax back to their global minimum energy structure and to provide an appropriate boundary condition. Since a layer of aluminum in our unit cell contains six atoms and requires nine oxygen atoms to maintain the stoichiometric ratio, 15 atoms on each outer surface of the model are kept frozen. Estimates of the GB sliding barriers are determined as the energy difference between the minimum and the maximum energy structure found along each path.

In addition to using rigid sliding translations as an initial guess from which to allow ion relaxation, we also examine an initial condition in which the outermost atoms are still held fixed as described above but the positions of all other atoms are determined initially by a uniform shear deformation followed by ion relaxation. We decided to explore this initial condition because we found that for small sliding displacements the final relaxed structure corresponded simply to a sheared structure. These additional initial conditions are only done along the lowest energy sliding paths, namely along the b vector. We find no evidence for shear deformations along the a vector, even for small displacements; therefore, shear initial conditions would not be appropriate for sliding along the a vector.

Once the GB sliding energy profiles are determined, we estimate sliding barriers for a large set of possible dopants. We select groups III and IV transition metals, the lanthanides gadolinium and neodymium, and an alkaline earth

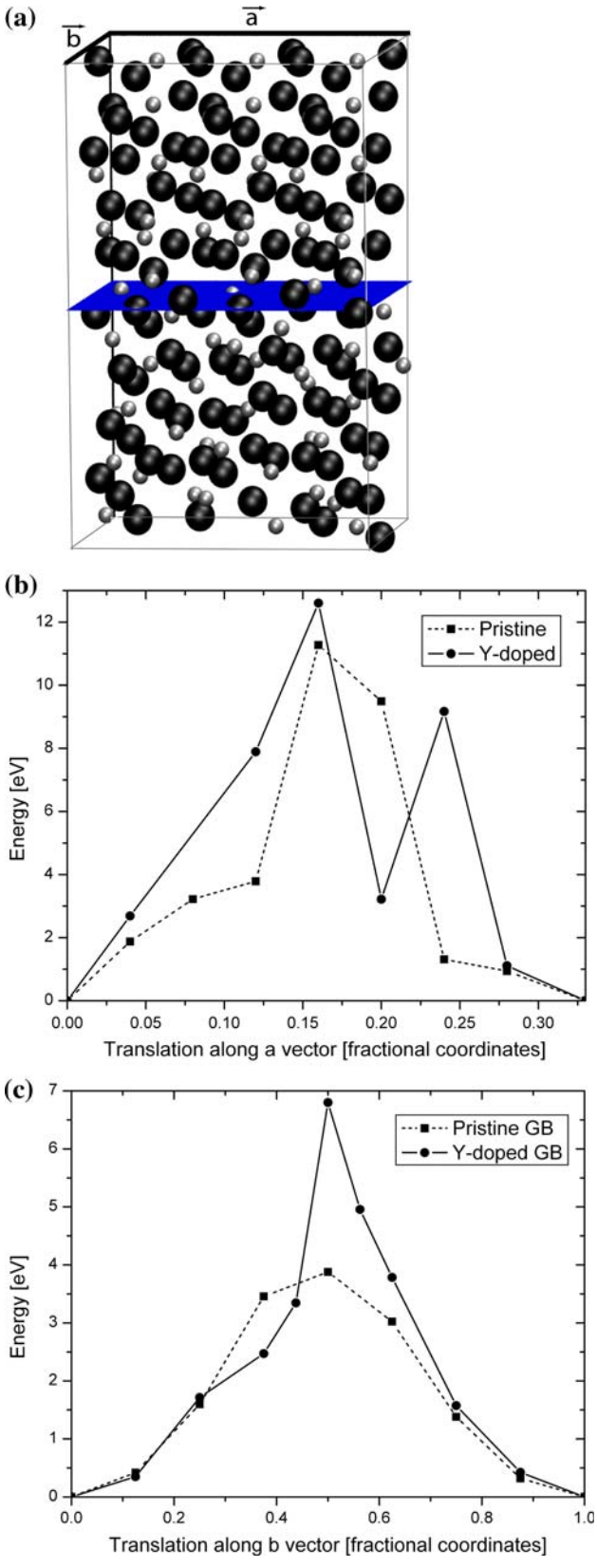

Fig. 1 The optimized structure of the pristine (undoped) alumina GB model used in this work is shown in (**a**). Oxygen atoms are represented in black, while aluminum atoms are in gray. The plane of the GB is also displayed. The GB sliding energy profiles are shown for the pristine and the Y-doped GBs along: (**b**) the *a* lattice vector and (**c**) the *b* lattice vector

(barium) as dopant candidates. Groups III and IV transition metals are commonly used as REs, while neodymium was first proposed by Harmer and coworkers [3] as a good creep inhibitor. We consider barium and gadolinium because both are large cations that make a large number of strong bonds to oxygen, based on known metal-oxo diatomic bond strengths [37] and their typical high coordination number in oxides.

Due to the prohibitive computational expense of this undertaking, we do not construct the entire sliding profile for each dopant. We assume that the substitution of the Y atom at the GB with a different dopant will affect the GB model minimum and maximum energy structures only locally. This assumption is based on findings from our previous work that, e.g., Y and Hf adsorption sites on the GB coincide almost perfectly, despite their difference in valency [34]. We therefore assume that using the lowest-energy adsite structure for Y as a starting guess for all other metal cations is a reasonable first approximation, since Groups III, IV, and lanthanide elements have the same valencies as Y and Hf. The GB sliding barriers for all dopants are obtained by using the minimum and maximum energy structures obtained for the Y-doped case along the *b* lattice vector, as it is the pathway with the much lower barrier. (We are interested in the most likely sliding pathway, which will be the one with the lowest energy barrier.) As a first approximation, the Y atom is substituted by the new dopant atom and the total energy is calculated for the maximum and minimum structures by allowing only the 40 closest atoms on each side of the GB to relax. The outermost 50 atoms on each outer surface of the GB are kept frozen in the positions found for minimum and maximum energy structures of the Y-doped GB. Once these first approximations to the doped GB structures are obtained, we perform a further relaxation of ions, but now only keeping the outermost 15 atoms on each outer surface frozen. Finally, we performed a test on the high energy structures for representative cases (the La-, Hf-, and Ba-doped GBs) to verify that they are indeed the highest energy structures along the profile. To do that, we translate one of the grains by approximately 0.5 Å with respect to the other one in each direction along the lattice vector, freeze the outermost 15 atoms on each outer surface of the model, and allow all the other atoms to fully relax. The

total energies of the resulting structures are verified to be lower than our best estimate for the highest energy structure.

Finally, changes in bonding across the GB interface for all the lowest and highest energy structures on the sliding profile are examined. The number of Al–O bonds at the GB interface is calculated and their average lengths are compared for the minimum and maximum energy structures along the sliding path for both pure and doped GBs. The number of bonds is determined by considering all pairs of atoms with interatomic distances less than 2.5 Å to be bonded. This distance allows for the inclusion of partial and elongated bonds that are still within the nearest-neighbor shell. In addition, the number of dopant–oxygen bonds formed and their average lengths are also calculated. The 2.5 Å cutoff for bond counting is used here as well, except for oxygen bonds to Nd, La, Gd, and Ba, for which we use a larger cutoff (2.75 Å) because of their larger ionic radii.

Results

GB sliding for pristine and Y-doped GBs

The energy profiles for sliding along the *a* and *b* lattice vectors of the pristine and Y-doped GBs are shown in Fig. 1b and c. In both cases, the highest energy structure appears at half of the total displacement length surveyed. The energy barrier for GB sliding along the lattice vector *a* for the pristine GB is predicted to be 11.3 eV, whereas the barrier for sliding along the shorter *b* vector is predicted to be much lower, 3.9 eV. This indicates that the *b* vector is the preferential direction of sliding during creep of this GB. Our value of 3.9 eV is certainly lower than but consistent with $\sim$5.0 eV barriers Harmer and coworkers measured for creep in polycrystalline alumina [3]. Of course, there is no reason that our barrier should match precisely those measured in a polycrystal with a wide variety of GB types.

Our barrier is considerably lower than the 9.8 eV predicted by Nakamura et al. for an alumina twin boundary [23]. Multiple explanations are possible for this large difference. First, the experimental value is derived from kinetic measurements on a polycrystalline alumina sample that contained a large number of asymmetric and high-angle GBs. Our value might be closer to what Harmer and coworkers measured because the GB model Nakamura et al. used was more symmetric than ours and thus somewhat less representative of the average GB. Indeed, twin boundaries are likely to have larger GB sliding barriers, simply because they are likely to have maximal bonding at the interface and hence sliding will be more difficult (more bonds to break costs more energy). Another contribution to the discrepancy might be their slightly different method used to obtain the sliding energy profile. They obtained each structure along their sliding pathway by translating the relaxed structure of the preceding point by fine increments. Theoretical zero Kelvin energy profiles for plastic deformations surely can produce results that do not match high-temperature measurements, since at zero Kelvin the system lacks the energy to overcome energy barriers and "jump" to a lower energy arrangement of atoms. Nakamura et al. might not have given the system enough energy to escape local minima and caused it to be stuck on a higher energy sliding pathway. To overcome this problem, Molteni et al. [38] performed sliding calculations in the reverse direction in their work on Ge GBs. They defined the intersections between the forward and backward curves as crossover points and used them as an approximation to the energy barrier. The sliding then was predicted to always follow the lower of the two energy curves, and the resultant energy barriers were much lower than what would be found by the method Nakamura et al. adopted. We took a slightly different approach by obtaining the points on the sliding energy curve by performing translations relative to the global minimum structure instead of the preceding structure along the sliding pathway. In this way, we have, in practice, enticed bond breaking at the GB interface, which resulted in breaking bonds at a smaller displacement and at lower energies.

As mentioned in the calculational details, we also considered shear deformations rather than rigid translations as a way to set up the initial conditions for sliding along the *b* vector. At small displacements of one grain with respect to the other, these two sets of initial conditions are found to give the exact same structures and energies. However, as the GB displacement approaches its peak energy, we see that shearing initial conditions lead to different structures and energies both for the pristine and Y-doped GBs. This is illustrated in Fig. 2, where we show that shearing the pristine GB from the two different minima produces structures around the midpoint displacement of 0.5 that are mostly higher in energy than the peak value found using the rigid translation as an initial condition. Thus while the initial GB sliding occurs via shear deformations, it is likely that the GB finds a way to traverse the sliding path involving translation rather than shear near the midpoint displacement, since this translation path has a lower energy. This makes physical sense that initial displacements would involve uniform shear up to a point where slip (essentially the equivalent of translation) will occur.

For the sliding of the Y-doped GB, we predict an energy barrier of 12.7 eV for sliding along the *a* vector and 6.8 eV for sliding along the *b* vector, based on rigid translation initial conditions (see Fig. 1b, c). Shearing initial conditions along the *b* vector showed that with Y present, it is possible to follow a lower energy shearing pathway prior to

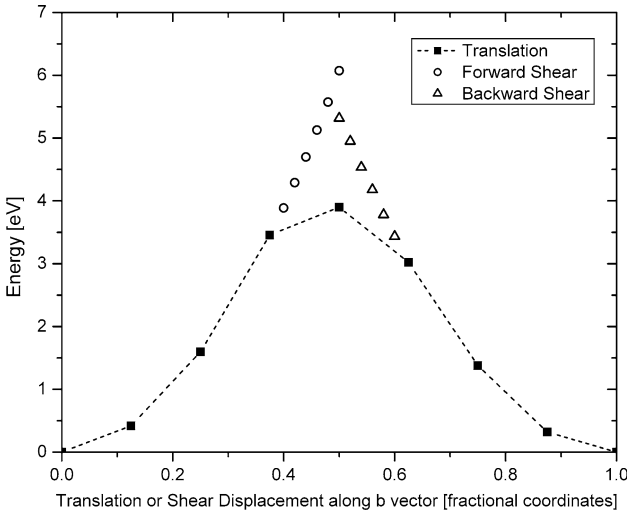

Fig. 2 GB sliding energy profiles for the pristine alumina GB along the *b* lattice vector, shown for initial conditions of rigid translation (squares) and uniform shear (circles and triangles) displacements from minimum energy structures at fractional coordinates 0.0 and 1.0. The lowest energy points below 0.375 and above 0.625 fractional coordinates are shown for rigid translation initial conditions, but uniform shear initial conditions lead to the same structures and energies. Only between 0.375 and 0.625 do the two sets of initial conditions lead to different energies and structures. The minimum energy path will thus consist of shear deformation from 0.0 followed by slip to traverse the barrier followed by shear deformation to reach the new minimum at 1.0

the peak in the energy profile, but ultimately the peak in Fig. 1c must be reached by translation (i.e., slip), so our best estimate for the barrier remains as reported above. Thus, as in the pristine GB, sliding along the *b* vector in the Y-doped GB is energetically favored over sliding along the *a* lattice vector.

Our calculations show that segregation of one atom of Y to the GB interface unit cell (equivalent to 1/6 monolayer, ML) significantly increases the energy barriers for sliding. Assuming that sliding occurs along the lowest energy path, i.e., along the *b* lattice vector, 1/6 ML of segregated Y atoms increases the energy barrier by 2.9 eV, as shown in Fig. 1c. Our results are consistent with the creep activation energies measured by Harmer and coworkers [3] for Y-doped alumina. They obtained creep activation energies of 7.3 and 7.1 eV for 100 and 1,000 ppm Y in alumina, respectively, increases of 2.3 and 2.1 eV over the undoped case. Although these Y concentrations sound low, they represent an average over the whole sample; concentrations of dopants at the GB interface are much higher, as it is energetically more favorable for Y atoms in alumina to segregate to GBs than to stay in the bulk [34]. In fact, high-resolution scanning transmission electron microscopy (HR-STEM) and extended X-ray absorption fine structure (EXAFS) experiments [39, 40] on alumina polycrystals indicate that Y can have a coverage at alumina GBs of up to 1/2 ML. Thus our structure with 1/6 ML Y is a reasonable model of Y concentrations at GBs in Y-doped alumina. The fact that the trend of greatly increased barriers upon Y-doping is reproduced well by our model lends credibility to its use to study trends for other dopants, as discussed in the next section.

The difference in sliding barriers between the pristine and Y-doped GBs can be understood by comparing the bonding at the GB interface for the minimum and maximum energy structures along the sliding pathway. By "maximum energy structure," we refer to the structure we estimate to correspond to the maximum energy along the lowest energy sliding pathway (along the *b* lattice vector). Table 1 contains the number of Al–O bonds across the GB and their average length for the pristine and each doped GB, as well as the total number of dopant–oxygen bonds and their average lengths. The pristine GB global minimum structure has 15 Al–O bonds across the GB interface and those bonds have an average length of 2.01 Å. The maximum energy structure's GB interface bonding profile is quite similar, with 15 Al–O bonds having an average length of 1.99 Å. This shows that all bonds that were stretched and broken during sliding were compensated by the formation of new bonds, keeping the net number and length constant.

The Y-doped GB exhibits significantly different behavior. The minimum energy structure for the Y-doped GB includes 9 Al–O bonds with an average length of 1.92 Å and 5 Y–O bonds with an average length of 2.32 Å. However, the maximum energy structure has a very different bonding layout. The number of Y–O bonds increases to 6 and the Y–O average length stays almost constant (2.33 Å), but the number of Al–O bonds falls to only 4. This large drop in the number of Al–O bonds upon sliding is only

Table 1 The number of Al–O bonds across the GB interface and their average length, *d*, in Å for all the minimum and maximum energy structures along the lowest energy sliding path, as well as the total number of dopant-oxygen (M–O) bonds and their average length, *d*

	Minimum energy structures				Maximum energy structures			
	# (Al–O)	*d*	# (M–O)	*d*	# (Al–O)	*d*	# (M–O)	*d*
Pristine	15	2.01	–	–	15	1.99	–	–
Y	9	1.92	5	2.32	4	1.82	6	2.33
Ba	10	1.92	5	2.58	4	1.85	6	2.59
La	9	1.92	5	2.44	4	1.83	6	2.44
Sc	9	1.92	5	2.10	4	1.82	6	2.20
Hf	10	1.92	5	2.16	4	1.82	6	2.16
Zr	11	2.03	5	2.24	4	1.82	6	2.19
Ti	11	1.99	4	2.03	4	1.81	5	2.01
Gd	9	1.93	5	2.36	4	1.82	6	2.38
Nd	9	1.92	5	2.42	4	1.82	6	2.42

partially compensated with a shortening of the remaining bonds by 0.1 Å. Therefore, at the highest energy point on the sliding energy profile, Y prevents the formation of new Al–O bonds across the GB interface that would compensate for the ones broken during sliding. This causes a net loss of bonding at the interface and an increase in the total energy, which in turn leads to a higher sliding energy.

GB sliding with other dopants at the GB

The predicted sliding energy barriers for GBs doped with a variety of other metal atoms are shown in Table 2. Interestingly, GB sliding energy barriers obtained using a model in which 100 outermost atoms (50 on each side) are frozen to the positions of the maximum energy structure along the Y-doped GB sliding pathway are virtually identical to the values given in Table 2, in which all but the outer 30 atoms were frozen. In all but the Ti-doped systems, decreasing the number of atoms kept frozen from 100 to 30 causes a change of only 0.1 eV in the GB sliding energy. The change for the Ti-doped GB was 0.3 eV. This suggests that generally only atoms in the first few layers nearest the GB are greatly affected by sliding.

All segregated dopants studied cause an increase in sliding barriers. The element producing the highest increase is barium, which usually forms 2+ ions. The sliding barrier for the GB doped with barium is predicted to be 8.1 eV, which is 1.3 eV larger than found for the Y-doped GB and 4.2 eV larger than the barrier of the pristine GB. The sliding barriers of scandium-, lanthanum-, neodymium-, and gadolinium-doped GBs are in the 6.7–6.9 eV range, very similar to the Y-doped GB. All of these elements form 3+ ions and produce similar sliding barriers. Likewise, the sliding barriers for elements that form 4+ ions (titanium, zirconium, hafnium) are also concentrated in a specific range, 5.2–6.0 eV, which is lower than for Ba-doped and Y-doped GBs, but still larger than the value for the pristine GB. Our predictions are consistent with available experimental trends for creep activation barriers in alumina doped with La and Zr, even agreeing to within 0.5 eV for Nd-doped alumina GBs [3]. This level of agreement is quite remarkable, considering that we are using one fairly simple GB to model an actual polycrystal that includes a large number of very disordered GBs.

Table 2 PAW-DFT-GGA GB sliding barriers and the experimental creep activation energies (in eV) [3]. The dopant concentration used was 1/6 ML in all simulations

Dopant	None	Ba	Nd	Sc	Y	La	Gd	Ti	Zr	Hf
This work	3.9	8.1	6.9	6.8	6.8	6.8	6.7	6.0	5.6	5.2
Expt.	5.0		7.4		7.1, 7.3	8.0, 8.3			7.3	

The bonding profiles at the interface of all doped GBs are very similar to what is observed for Y. Table 1 shows that most of the minimum energy structures of the doped GBs have 9 Al–O bonds across their interfaces, with an average length of 1.92 Å, which is the average bond length in bulk α-alumina. The exceptions are the Hf- and Ba-doped GBs that have 10, and Ti- and Zr-doped GBs that have 11, Al–O cross-boundary bonds. However, the additional cross-boundary bonds in the Hf-, Ti-, and Zr-doped GBs are larger than 2.45 Å; such long "bonds" are likely to be weak. This is not the case with Ba-doped GB, with 10 Al–O bonds of average length 1.92 Å.

The number and average length of dopant–oxygen bonds for the minimum energy structures of the doped GBs are also given in Table 1. In all minimum energy structures of doped GBs, the dopants formed bonds with five oxygen atoms, except for Ti, which formed four such bonds.

The bonding at the interfaces of all doped GB "maximum energy" structures (our estimates for the sliding transition state structures) is again very similar to Y's. In all cases, the dopants' coordination number increases by one, i.e., all dopants are hexa-coordinated, except for Ti which is penta-coordinated like Y. The average length of the dopant–oxygen bonds changes by at most a few picometers. On the other hand, the number of Al–O bonds in all cases decreases to four and their average length shortens to 1.82 Å. Thus, just as for Y-doped GBs, the net number of bonds across the interfaces decreases by at least four in all cases, as the structures undergo GB sliding. These findings demonstrate that all dopants, independent of their preferred ionic charge and radius, have the same effect on the bonding at the GB interface during GB sliding. Their presence inhibits the GB's ability to conserve the number of bonds across the GB interface during GB sliding. Thus, the decreased number of bonds across the interface upon sliding destabilizes the doped GB, thereby inhibiting sliding.

Our calculations do not permit us to draw clear conclusions on why metals that form 3+ ions lead to higher GB sliding barriers than those that form 4+ ions, or why the addition of Ba results in the highest GB sliding energy. We speculate that the larger the ionic radius of the segregated atom, the more energy it takes for aluminum cations to rearrange themselves around it and form new bonds with oxygen ions across the GB interface. The rationale is as follows. Since the interface of our model GB consists of alternating Al and O ions, bonds are broken and like-charged ions approach each other as the one side of the interface slides against the other. The repulsion between the like-charged ions induces a short-range rearrangement of ions in an attempt to reform the broken bonds across the interface. When a large cation is present at the GB interface, it inhibits the short-range restructuring by greatly repelling Al ions and by constraining the positions of O ions at the

interface by bonding to them. As long as breaking dopant–oxygen bonds costs more energy than breaking Al–O bonds, it is more likely that Al atoms will have to rearrange themselves around the dopant–oxygen "cluster" than vice versa. Taking metal–oxygen bond enthalpies from diatomic molecules as an approximate measure for bond strength in solid oxides, the metal–oxygen bonds formed by the dopants studied are all stronger than those formed by aluminum [37]. Thus, we expect to see an increase in GB sliding energy barrier after the segregation of any dopant. Ba, which has the largest ionic radius, forms the weakest bonds with oxygen out of all dopants (though still stronger than Al), and yet produces the highest GB sliding energy. Hence, we can conclude that the dominant feature influencing the height of the energy barrier is the size of the ionized dopant and its affect on the local rearrangements of Al–O bonds across the GB interface.

Conclusions

We have performed periodic DFT-GGA calculations on the pristine and metal-doped $\Sigma 11(10\bar{1}1)\|(10\bar{1}\bar{1})$ α-alumina GB to investigate the effects of reactive elements on GB sliding. We find that all doped α-alumina GBs have larger GB sliding barriers than the pristine GB. The predicted trends in GB sliding barriers are uncannily consistent with measured creep activation energies by Harmer and coworkers, suggesting that GB sliding most definitely contributes to creep in alumina.

The magnitude of the increase in sliding energy is found to depend on the ionic radii of the dopants. This effect was shown to be related to the number of bonds formed across the GB interface. In the pristine GB case, the number of Al–O bonds across the GB is the same in both the minimum and maximum energy structures along the sliding pathway. By contrast, the doped GBs show a net loss of bonding during sliding. Compared to the minimum energy structures, the structures approximating a sliding transition state have at least four less bonds across the GB interface. We find that an element that forms 2+ ions leads to a larger sliding barrier than dopants that form 3+ ions, which in turn produce a larger sliding barrier than dopants that form 4+ ions. In general, the dopants with larger ionic radii produce larger sliding energies. Since the decrease in bonding is attributed to the loss of exclusively Al–O bonds, we speculate that the larger the dopant cation, the more energetically difficult it is for the aluminum cations to rearrange themselves around the dopant to re-establish the original bond count across the GB.

Of course, the total creep rate depends on the rates of GB sliding and Coble (diffusion) creep. Since both occur simultaneously, the observed creep rate is determined by the fastest of the two mechanisms. In principle, dopants can have a large inhibiting effect on GB sliding, but if the dopant does not prevent diffusion of aluminum and oxygen atoms along the GB, its overall performance as creep inhibitor could be poor. The ideal dopant has to be able to inhibit both GB sliding and serve as an effective inhibitor of Coble creep diffusion. In other work [34, 41], we have found that Y and Hf indeed are effective diffusion inhibitors via site-blocking, suggesting that the same elements should reduce both forms of creep. As noted above, we predict that barium is the most effective GB sliding inhibitor among the metal dopants thus far considered. Whether Ba also inhibits diffusion of Al and O along GBs remains to be determined.

Finally, we acknowledge that our model GB is a simple one, and similar studies should be performed on less symmetric GBs to determine if the current predictions are robust with respect to GB structure. Moreover, even for this GB, we cannot exclude the existence of additional sliding pathways, which lends uncertainty to the energetics and suggests that only the trends as a function of dopant should be trusted. However, we contend that although additional pathways with different activation barriers are likely to exist, they should not affect our qualitative conclusions on the role of REs in GB sliding nor the trends as to which REs are most effective at inhibiting creep dominated by GB sliding. Indeed, the qualitative agreement with Harmer and coworkers' measurements gives us hope that our current predictions will hold true for other GBs as well.

Acknowledgements We are grateful to the Air Force Office of Scientific Research for financial support, to the NAVO and ERDC DoD high performance computing centers for supercomputing time, and to Drs. Berit Hinnemann and Ashwin Ramasubramaniam, and Prof. Nicholas Mosey for helpful discussions.

References

1. Padture NP, Gell M, Jordan EH (2002) Science 296:280
2. Evans AG, Mumm DR, Hutchinson JW et al (2001) Prog Mater Sci 46:505
3. Cho J, Wang M, Chan HM et al (1999) Acta Mater 47:4197
4. Cho J, Wang M, Chan HM et al (2001) J Mater Res 16:425
5. Coble RL (1963) J Appl Phys 34:1679
6. Lifshitz IM (1963) Sov Phys JETP 17:909
7. Haynes JA, Ferber MK, Porter WD et al (1999) Oxid Met 52:31
8. Langdon TG (1970) Philos Mag 22:689
9. Ashby MF, Verrall RA (1973) Acta Met 21:149
10. Nieh TG, Wadsworth J (1990) Annu Rev Mater Sci 20:117
11. Ruano OA, Wadsworth J, Sherby OD (2003) Acta Mater 51:3617
12. Rachinger WR (1952–53) J Inst Met 81:33
13. Langdon TG (2006) J Mater Sci 41:597. doi:10.1007/s10853-006-6476-0
14. Pint BA, Hobbs LW (1994) Oxid Met 41:203
15. Kottada RS, Chokshi AH (2000) Acta Mater 48:3905
16. Bedu-Amissah K, Rickman JM, Chan HM et al (2007) J Am Ceram Soc 90:1551

17. Cheng H, Dillon SJ, Caram HS et al (2008) J Am Ceram Soc 91:2002
18. French JD, Zhao JH, Harmer MP et al (1994) J Am Ceram Soc 77:2857
19. Matsunaga K, Nishimura H, Muto H et al (2003) Appl Phys Lett 82:1179
20. Chokshi AH (1990) J Mater Sci 25:3221. doi:10.1007/BF00587678
21. Heuer AH (2008) J Eur Ceram Soc 28:1495
22. Veal BW, Paulikas AP, Hou PY (2007) Appl Phys Lett 90:121914
23. Nakamura K, Mizolguchi T, Shibata N et al (2007) Phys Rev B 75:184109
24. Hohenberg P, Kohn W (1964) Phys Rev 136:B864
25. Kohn W, Sham LJ (1965) Phys Rev 140:A1133
26. Kresse G, Hafner J (1993) Phys Rev B 48:13115
27. Kresse G, Fürthmüller J (1996) Phys Rev B 54:11169
28. Kresse G, Fürthmüller J (1996) Comput Mater Sci 6:15
29. Blöchl PE (1994) Phys Rev B 50:17953
30. Kresse G, Joubert D (1999) Phys Rev B 59:1758
31. Perdew JP, Burke K, Erzerhof M (1996) Phys Rev Lett 77:3865
32. Monkhorst HJ, Pack JD (1976) Phys Rev B 13:5188
33. Hinnemann B, Carter EA (2007) J Phys Chem C 111:7105
34. Milas I, Hinnemann B, Carter EA (2008) J Mater Res 23:1494
35. Kenway PR (1994) J Am Ceram Soc 77:349
36. Höche T, Kenway PR, Kleebe HJ et al (1994) J Am Ceram Soc 77:339
37. Lide DR (ed) (1999) CRC handbook of chemistry and physics, 79th edn. CRC Press, Boca Raton, Florida
38. Molteni C, Francis GP, Payne MC et al (1996) Phys Rev Lett 8:1284
39. Voytovych R, MacLaren I, Gülgün MA et al (2002) Acta Mater 50:3453
40. Wang CM, Cargill GSIII, Chan HM et al (2000) Acta Mater 48:2579
41. Milas I, Hinnemann B, Carter EA, to be published